Optimizing Multiscale Networks for Transient Transport in Nanoporous Materials

Robert H. Nilson and Stewart K. Griffiths

Physical and Engineering Sciences Center
Sandia National Laboratories, P. O. Box 969, Livermore CA 92007
rhnilso@sandia.gov and skgriff@sandia.gov

ABSTRACT

Hierarchical nanoporous materials afford the opportunity to combine the high surface area and functionality of nanopores with the superior charge/discharge characteristics of wider transport channels. In the present paper we optimize the apertures and spacing of a family of transport channels providing access to a surrounding nanoporous matrix during recharge/discharge cycles of materials intended for storage of gas or electric charge. A diffusive transport model is used to describe alternative processes of viscous gas flow, Knudsen gas flow, and ion diffusion. The coupled transport equations for the nanoporous matrix and transport channels are linearized and solved analytically for a periodic variation in external gas pressure or ion density using a separation-of-variables approach in the complex domain. Channel apertures and spacing are optimized to achieve maximum inflow/outflow from the functional matrix material for a fixed system volume.

Keywords: nanoporous materials, hierarchical, network optimization, nanofluidics, nanoscale transport

1 INTRODUCTION

Nanoporous materials are finding increased use in a range of emerging technologies including hydrogen and methane storage, supercapacitors, desalination membranes, and fuel cell membranes. In these applications, nanoscale pores provide high surface area as well as functionality but may also inhibit device-scale transport needed to rapidly charge and discharge the medium. The opposing goals of nanopore functionality and rapid transport can both be achieved, however, using hierarchical materials having nanopores interconnected with larger-scale transport channels.

Previous work on nanoporous materials has been largely focused on synthesis, material characterization, and measurements of functionality. Modeling of nanopore transport is largely concerned with single-pore processes, while related modeling of network transport has been addressed mainly in other disciplines with the goal of minimizing global flow resistance under steady-flow conditions [1,2,3]. In contrast, we seek to maximize inflow/outflow volumes under transient conditions where flow resistance, capacitance, and desired discharge time are all important.

2 GOVERNING EQUATIONS

Consider a highly idealized nanoporous material comprised of permeable matrix slabs separated by an array of parallel planar channels having uniform aperture and spacing, a_1 and b_1, as illustrated schematically in Fig. 1. The nanopores within the slabs have a characteristic aperture and spacing of a_0 and b_0, bulk porosity of $\phi_0 = a_0 / b_0$, and internal diffusivity of D_0. The nanoporous slabs might alternatively be characterized in terms of their bulk transport properties, such as permeability and porosity, and a characteristic nanopore dimension, a_0, without requiring explicit knowledge of pore morphology.

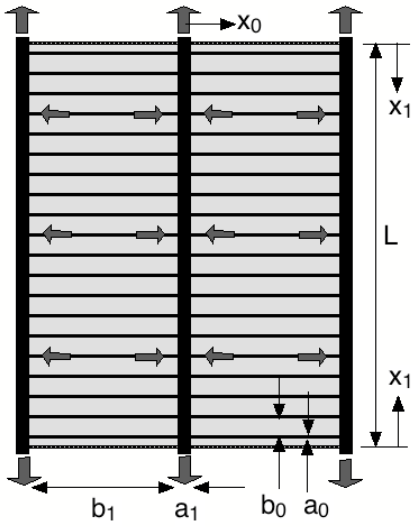

Figure 1: Geometry of multiscale network.

Gas flow or diffusion within the porous matrix slabs can generally be described by a diffusion equation of the form

$$\phi_0 \frac{\partial \rho_0}{\partial t} = \frac{\partial}{\partial x_0}\left(D_0 \frac{\partial \rho_0}{\partial x_0} \right) \qquad (1)$$

where ρ is the density, t is time, x_0 is distance from the slab surface, and D_0 is the diffusion coefficient. In gas transport, ρ is the molar density of the gas and the diffusion

rate is limited by collisions among gas molecules and by collisions with pore walls. When the mean free path is small compared to lateral channel dimensions, collisions among gas molecules predominate and $D_0=\kappa P/\mu$ where κ, P, and μ, are the permeability, pressure, and viscosity. However, in nanoscale pores, the mean free path of the gas is often small compared to the pore dimension. In this instance the appropriate diffusivity is given by the Knudsen expression, $D_0=va_0$ in which v is the mean thermal speed. The same model applies in an approximate manner to the porous electrodes of supercapacitors where, ρ is the charge density of the electrolyte within the pores and D_0 is the effective ion diffusivity or mobility.

Transport along the open vertical channels in Fig. 1 is governed by an equation that resembles Eq. (1) but also includes lateral transport between the channels and the adjacent permeable slabs.

$$\phi_1 \frac{\partial \rho_1}{\partial t} = \frac{\partial}{\partial x_1}\left(D_1 \frac{\partial \rho_1}{\partial x_1}\right) + \frac{2D_0}{a_1}\frac{\partial \rho_0}{\partial x_0}\bigg|_{x_0=0} \qquad (2)$$

Here, x_1 is measured from the bottom inflow/outflow surface and the factor of $2/a_1$ in the last term represents the ratio of surface to cross-sectional area for a rectangular channel. Since the transport channels are typically assumed to be open, the porosity ϕ_1 will be taken as unity. Also, the gas diffusivity is given by $D_1 = P a_1^2/12\mu$ or by $D_1=va_1$ for the viscous and Knudsen regimes, respectively. Thus, wider channels have higher diffusivities. Similarly, the ion transport diffusivity D_1 along wider channels will sometimes exceed D_0 because $a_1>a_0$, reducing the effects of hindered diffusion in nanoscale pores. To facilitate analytical solution we will assume that the diffusion coefficients D_k are constant and we define the diffusivity as $\alpha_k = D_k/\phi_k$ for k=0, 1.

To approximate the discharge/recharge cycle of an energy storage material we seek solutions of the following form appropriate for a sinusoidal variation in the external density having an amplitude and mean of $\Delta\rho$ and ρ_r.

$$\rho^* = \frac{\rho-\rho_r}{\Delta\rho} = e^{i\omega t}\,\rho_0^*\left(x_0^*\right)\rho_1^*\left(x_1^*\right) \qquad (3)$$

Here, $\rho_0^*(x_0^*)$ represents the variation of ρ^* within the matrix slabs, $\rho_1^*(x_1^*)$ is the variation along transport channels, $x_0^* = 2x_0/b_1$, $x_1^* = 2x_1/L$, and $i \equiv \sqrt{-1}$. Substitution of this assumed form into Eq. (1) yields a second order ordinary differential equation for $\rho_0^*(x_0^*)$

$$i\,\lambda_0^2\,\rho_0^* = \frac{d^2\rho_0^*}{dx_0^{*2}} \qquad (4)$$

subject to the boundary condition $\rho_0^* = 1$ at the interface between channels and slabs where $x_0^* = 0$ and the symmetry condition $(\rho_0^*)' = 0$ at the slab midplane where $x_0^* = 1$. The solution is

$$\rho_0^* = \frac{\cosh\lambda_0\sqrt{i}\left(1-x_0^*\right)}{\cosh\lambda_0\sqrt{i}} \quad \text{where} \quad \lambda_0 \equiv \frac{b_1}{2}\sqrt{\frac{\omega}{\alpha_0}} = b_1^* \qquad (5)$$

The Fourier modulus λ_0 indicates the ratio of the cross-slab diffusion time, $\tau \sim (b_1/2)^2/\alpha_0$, to the discharge cycle time, $\tau\sim 1/\omega$. Similarly, substitution of Eqs. (3,5) into Eq. (2) yields the following result for the transport channels.

$$\rho_1^* = \frac{\cosh\hat{\lambda}_1\sqrt{i}\left(1-x_1^*\right)}{\cosh\hat{\lambda}_1\sqrt{i}} \qquad (6)$$

$$\hat{\lambda}_1 = \lambda_1\left[1+\frac{\phi_o b_1^*}{a_1^*}\frac{\tanh\lambda_0\sqrt{i}}{\lambda_0\sqrt{i}}\right]^{1/2} \qquad (7)$$

$$\lambda_1 = \frac{L}{2}\sqrt{\frac{\omega}{\alpha_1}} = \frac{L}{2}\sqrt{\frac{\omega}{\alpha_0}}\left(\frac{\alpha_0}{\alpha_1}\right) = L^*\left(\frac{\alpha_0}{\alpha_1}\right) = L^*\left(\frac{a_0^*}{a_1^*}\right)^m \qquad (8)$$

Here, a* and b* and L* have all been normalized by the length scale $\sqrt{4\alpha_0/\omega}$ which also appears in the Fourier moduli, λ_0 and λ_1.

The exponent m appearing in Eq. (8) describes the variation of diffusivity, $\alpha = D/\phi$, with channel aperture, a. As explained earlier, m=2 for a viscous gas flow, m=1 for free molecular gas flow, and m=0 for a simple diffusion process. However, since the surface to volume ratio is 2/a in rectangular channels, each of these exponents will be increased by unity in cases where the capacitance, ϕ, of the channel is associated mainly with the channel surface area, rather than the channel volume. This is often the case in nanoporous gas storage materials where surface adsorption provides the primary capacitance and in supercapacitor devices where electric charge is accumulated in electric double layers having a thickness of one or two molecular diameters. Thus, our example calculations will explore the range $1<m<3$. We exclude m=0, because in this case wider transport channels provide little benefit.

The pore structure is optimized by adjusting the values of a_1^* and b_1^* to obtain the maximum cyclical inflow/outflow from the nanopores subject to a given system volume. Maximizing cyclical flow is equivalent to maximizing the amplitude of the sinusoidal variation in the mean nanopore density, $\left|\Delta\overline{\rho}_0^*\right|$. This quantity is readily evaluated by spatial integration of the solution given by Eqs. (3, 5-8) over the nanopore volume.

$$\left|\Delta\bar{\rho}_0^*\right| = \mathrm{mod}\left[\frac{\tanh\lambda_0\sqrt{i}}{\lambda_0\sqrt{i}}\,\frac{\tanh\hat{\lambda}_1\sqrt{i}}{\hat{\lambda}_1\sqrt{i}}\right] \qquad (9)$$

Because the smallest scale nanopores generally provide functionality or capacitance unavailable in wider transport channels, we will take credit only for density changes within the nanoporous matrix blocks. Thus, the optimization criterion, Ω, is taken as the product of $\left|\Delta\bar{\rho}_0^*\right|$ with the ratio of nanopore volume to total system volume.

$$\Omega = \left|\Delta\bar{\rho}_0^*\right|\,\frac{V_{nanopores}}{V_{total}} = \left|\Delta\bar{\rho}_0^*\right|\,\frac{\phi_0}{\phi_0 + a_1^*/b_1^*} \qquad (10)$$

Note that increases in a_1^* or decreases in b_1^* help to increase the numerator $\left|\Delta\bar{\rho}_0^*\right|$ in Eq. (10) but they also tend to increase the denominator. As a result, Ω has a maximum value for particular choices of a_1^* and b_1^*.

3 RESULTS

Figure 2 illustrates the variation of optimized channel apertures and spacing with normalized system scale. As the scale or frequency becomes larger, the optimal channel apertures and spacing both increase. Although it is relatively obvious that channel apertures would have to increase to maintain necessary transport, increased spacing might not have been anticipated. The wider spacing is apparently needed to avoid the allocation of excessive system volume to transport channels rather than nanopore functionality.

The nearly constant slopes on the logarithmic plot in Fig. 2 indicate power-law variations of the channel dimensions with system scale.

$$b_1^* = B\,L^{*p} \quad \text{and} \quad a_1^* = A\,L^{*q} \qquad (11)$$

The powers p and q depend upon m but not on a_0^*. It is quite surprising to see that these power-law relationships remain valid for relatively large values of the Fourier moduli and that they continue to hold even as the channel apertures approach the channel spacing for the case of m=1.

The Fourier moduli, λ_0 and $\hat{\lambda}_1$, are displayed in Fig. 3. As seen in Eq. (9), the quantities $\tanh(\lambda\sqrt{i})/(\lambda\sqrt{i})$ represent the fractional decreases in density amplitude within the pores and along the transport channels. Thus, the observed equality of the optimal moduli for m=2 indicates that the two scales of transport have equal impedance. For other values of m, the two moduli are comparable but not exactly equal. In all cases, the optimal moduli both increase in magnitude as the scale of the system increases, indicating greater impedance and greater reduction in density amplitude.

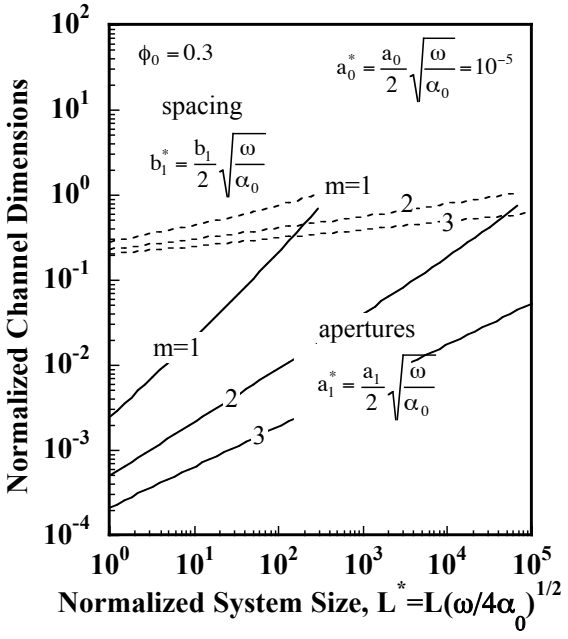

Figure 2: Variation of optimized channel apertures (solid lines) and channel spacing (dotted lines) with system scale. Parameter m describes the variation of transport diffusivity with aperture, $\alpha = D/\phi \sim a^m$.

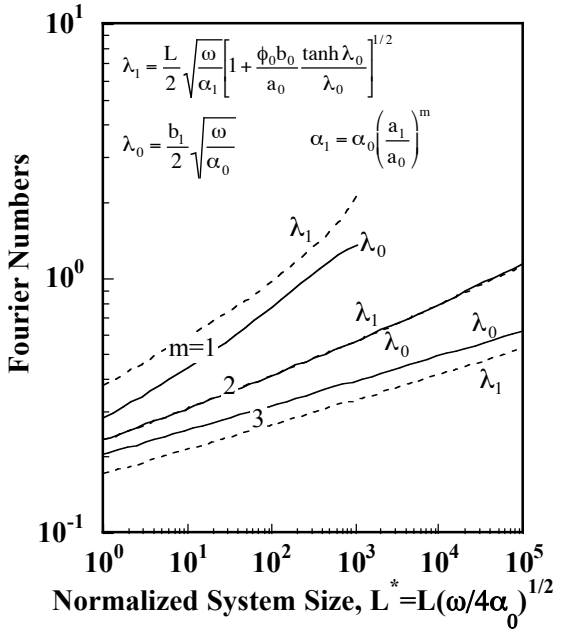

Figure 3: Fourier moduli indicate ratio of transport time to discharge cycle time for nanochannels, λ_0, and transport channels, $\hat{\lambda}_1$. Optimized moduli for the two scales are comparable but not always identical.

Figure 4 depicts the variation of the optimal transport efficiency, Ω, with normalized system scale. A value of Ω =1 indicates that the density within nanopores precisely tracks the imposed external density variation and that the volume lost to the transport channels is negligible. For m=3, $\Omega > 0.95$ for $L^*<10^5$, indicating great success in facilitating transport. The results are less impressive for m=1,2 because wider apertures provide less benefit when m is smaller.

Even in the most challenging case with m=1, $\Omega > 0.7$ for $L^*<10^2$. In this instance, the transport efficiency begins to fall off very sharply for $L^*>10^3$. This is because the channel apertures are becoming nearly as wide as the channel spacing, as clearly apparent in Fig. 2. For this reason, we did not extend the curves beyond this point.

The uppermost curves in Figure 5 provide a direct indication of the benefit derived by introduction of the transport channels.

$$R \equiv \frac{\Omega_{\text{with channels}}}{\Omega_{\text{without channels}}} \quad \text{where} \tag{12}$$

$$\Omega_{\text{without channels}} = \text{mod}\left[\frac{\tanh L^* \sqrt{i}}{L^* \sqrt{i}}\right] \tag{13}$$

For large values of L*, $\tanh L^* / L^* \to 1/L^*$ such that $R \to L^*$ so long as Ω remains near unity. Even in the worst case of m=1, R=50 for L*=100, indicating a level of discharge performance 50 times better than would have been obtained in the absence of transport channels.

4 SUMMARY

Channel apertures and spacing have been optimized through analytical modeling of diffusion transport in a hierarchical network having transport channels that provide access to nanoscale pores. The model is applicable to viscous gas flow (m=2) and Knudsen gas flow (m=1) as well as ion transport (m=0). These exponents increase by unity when most of the capacitance is associated with channel surfaces. For optimized systems, the impedance of transport channels is similar to that within pores. This observation can be used together with given analytical expressions to compute channel dimensions that maximize transport for prescribed system scales and discharge times.

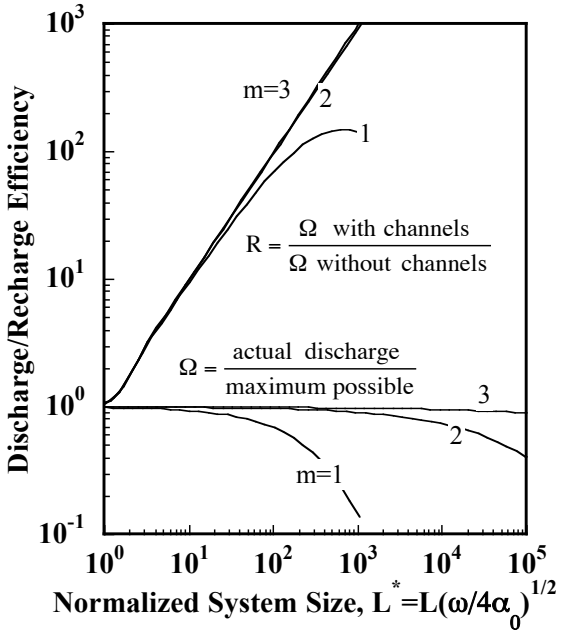

Figure 4: Transport efficiency Ω indicates optimized amount of discharge from nanopores relative to the maximum that might be achieved if nanopore density (or pressure) precisely tracked applied external conditions and if all of the system volume consisted of functional nanoporous material.

REFERENCES

[1] G. B. West, J. H. Brown, and B. J. Enquist, "A general model for the origin of allometric scaling laws in biology," Science 276, 122-126, 1997.

[2] M. Durand, "Architecture of optimal transport networks," Phys. Rev. E **73**, Article No. 016116, 2006.

[3] A. Bejan and S. Lorente, "Constructal theory of generation and configuration in nature and engineering," J. Appl. Phys. **100**, (4), Article No. 041301, 2006.

ACKNOWLEDGMENT

Sandia is a multiprogram laboratory operated by Sandia Corporation, a Lockheed Martin Company, for the United States Department of Energy's National Nuclear Security Administration under contract DE-AC04-94AL85000.